On the Possibility of Radar Detection of Ultra-high Energy Cosmic Ray- and Neutrino-induced Air Showers

Peter W. Gorham
Jet Propulsion Laboratory, Calif. Inst. of Technology
4800 Oak Grove, Drive, Pasadena, CA, 91109 USA

November 16, 1999

ABSTRACT

We show that cosmic rays air showers resulting from primaries with energies above 10^{19} eV should be straightforward to detect with radar ranging techniques, where the radar echoes are produced by scattering from the column of ionized air produced by the shower. If our analysis is correct, such systems could provide highly complementary measurements of air showers detected in existing and planned ground arrays such as the Auger Project, and crucial additional information for planned space missions such as OWL/Airwatch.

1. Introduction

Extensive air showers (EAS) resulting from primary cosmic-ray particles of energies above $\sim 10^{19}$ eV produce an ionization trail which is comparable to that of micro-meteors, which have been detected for many decades using radar methods (Lovell 1948; Greenhow, 1952; Hanbury Brown & Lovell 1962). EAS ionization trails are now commonly detected by their fluorescence emission at visible wavelengths (cf. Baltrusaitas et al. 1985). Future large EAS detector arrays such as the Auger project (Guérard et al. 1998) and the proposed space mission OWL/Airwatch (Scarsi et al. 1999; Krizmanic et al. 1999) have made fluorescence detection of EAS a centerpiece of their approach, since it can provide information such as the position of the shower maximum and the total shower energy which are often difficult to pin down with particle detectors alone. One of the most compelling reasons to extend the sensitivity of EAS detectors in this energy regime is the possibility that neutrinos of energy $\geq 10^{19}$ eV may be an important component of the primary particles (Capelle et al. 1999). Yet to our knowledge no one has yet attempted to study the ionization trail of these events using radar echo techniques, although as we will show here, the signals should be clearly detectable using standard methods used in studying meteors for decades.

Meteor ionization trails are commonly parameterized in terms of their ionization line density α (electrons m^{-1}), a measure of the total ionization content divided by the length of the meteor track. Typical radar-detected meteors occur at heights of 80–120 km, and have line densities of $\alpha = 10^{13}$ to 10^{16} m^{-1}. At the lowest detectable line densities, the incident meteor can have a mass

of 10^{-9} kg or less, with radii less than 100 μm. At typical velocities of $\sim$ 30 km s^{-1}, the implied kinetic energy of these meteor grains is 0.5 Joules or more, much of which goes into ionization of the air along it path.

A cosmic ray proton of energy 10^{19} eV has a kinetic energy also of order 1 J, and much of this energy also ultimately ends up in the form of ionization and excitation of atoms of the air along the path of the shower of charged particles that results from the proton's collision with nuclear hadrons. The primary differences between the meteor track and cosmic ray EAS are in the way the ionization column forms, and in the resulting ionization density profile.

For the meteor, ablation of material from its surface yields atoms with kinetic energies of $10^2 - 10^3$ eV, which ionize air molecules by direct collision with a mean free path of several cm. This yields an ionization column with an approximately Gaussian distribution of cross-sectional density, and an initial radius of order 1 m or less. The density then evolves with time due to diffusion from convective processes, bulk motions of the air, and the Lorentz forces of the ambient electric and geomagnetic fields. Recombination also eventually plays a role, though not a dominant one. At radar frequencies in the VHF range (30-100 MHz), echoes from typical meteors may be detectable for several seconds after the meteor is gone.

The ionization in an EAS, in contrast, is not produced by a single body, but rather by the collective effects of the disk highly energetic particles (mostly electrons and positrons) that make up the body of the shower. Because the lateral distribution of these particles spreads out as the shower progresses, the ionization column has a different initial distribution than that of a meteor, reflecting the evolution of the cross-sectional charged particle density. However, since the shower propagates essentially at the speed of light, it appears almost instantaneously compared to even the fastest meteors at $\sim$ 100 km s^{-1}.

An important measure of the transverse charged particle distribution in an EAS is the Moliere radius r_m within which of order 90% of the charged particles can be found. For air at sea level, $r_m \sim$ 70m, but it is important to note that within r_m the radial distribution is a power law, and many showers retain a tight core of particles of diameter several m or less.

2. Radar detection of ionization columns

For radar detection of the columns that result from either meteors or EAS events, there are two regimes to consider, depending on the plasma frequency ν_p of the ionized region: $\nu_p = (\rho_e^2/\pi m_e)^{1/2} \simeq 8.98 \times 10^3 \sqrt{\rho_e}$ where ρ_e is the electron density in cm^{-3}. These two regimes are known in the meteor radar community as the under- and over-dense regimes, respectively, and traditionally are divided at the line density of $\alpha \simeq 10^{14}$ m^{-1}. For our purposes, we distinguish them only on the basis of the ratio of radar to plasma frequency.

2.1. Underdense regime

For radar frequencies well below ν_p, the electrons within the ionization column scatter independently according to the Thomson cross section $\sigma_{Th} = (8\pi/3)(e^2/m_e c^2)^2 = 6.65 \times 10^{-29}$ m^2. The total effective radar backscatter cross section σ_b will then depend on the individual phase factors of each of the scattering electrons. For wavelengths that are larger than about 4 times the column diameter and angles that are nearly perpendicular to the track, the electrons scatter coherently over a region of the track $L = \sqrt{\lambda R/2}$ where R is the perpendicular distance to the track and λ the radar wavelength. This region of the track is known as the first Fresnel zone of the track, and the total radar backscatter cross section then becomes

$$\sigma_b = N_e^2 \sigma_{Th}, \tag{1}$$

where $N_e = \alpha L = \alpha\sqrt{\lambda R/2}$ is the number of electrons within a single Fresnel zone along the track. The radar cross section depends of the square of the electron density because of the assumption of full coherence.

For tracks where the radar frequency is below ν_p, but the wavelength is small compared to the diameter of the ionized column, the assumption of coherent scattering is no longer satisfied, and the individual phase factors of the electrons must be included. For this case the effective radar cross section can be written (Wehner 1987):

$$\sigma_b(\mathbf{k}) = \left| \int \sqrt{\rho_e^2(\mathbf{r}')\ \sigma_{Th}} \exp(2\ i\ \mathbf{k}\cdot\mathbf{r}') d^3\mathbf{r}' \right|^2 \tag{2}$$

where $\mathbf{r}' = \mathbf{R} - \mathbf{r}$ with $\mathbf{R}$ the vector impact parameter; $\mathbf{k}$ is the wavevector of the incident field ($k = 2\pi/\lambda$), $\mathbf{r}$ is the distance from the perpendicular point along the track to the point at which the electron density $\rho(\mathbf{r}')$ is evaluated, and $|\mathbf{R}| \gg |\mathbf{r}|$. Note that the argument of the exponential here includes an extra factor of two to represent the two-way phase. The term $\sqrt{\rho_e^2(\mathbf{r}')\ \sigma_{Th}}$ represents the differential contribution to the scattered electric field of a volume element of electrons which scatter coherently.

If we now write $\mathbf{q} = 2\mathbf{k}$ then equation 2 becomes

$$\begin{aligned} \sigma_b(\mathbf{q}) &= \sigma_{Th} \left| \int \rho_e(\mathbf{r}') \exp(i\mathbf{q}\cdot\mathbf{r}') d^3\mathbf{r}' \right|^2 \\ &= \sigma_{Th} \left| FT(\rho_e(\mathbf{r}')) \right|^2 \end{aligned} \tag{3}$$

where $FT(\rho_e(\mathbf{r}'))$ denotes the Fourier transform of the electron density.

Equation 3 thus reduces the problem of estimating the effective cross section in the underdense case to that of calculating the Fourier power spectral density of the electron density distribution.

2.2. Overdense regime

When the electron density $\rho_e(r)$ produces a surface where the plasma frequency exceeds the frequency of the incident radiation at some critical radius r_c from the track, the resulting index of

refraction becomes imaginary, and total external reflection of the radiation occurs. Under these conditions, the surface at r_c can be treated to first order as a metal cylinder, and the radar cross section is accordingly greatly enhanced, since the reflection becomes specular over a large portion of the physical area of the column, and the usual R^{-4} dependence of radar return power no longer applies. When $r_c \gg \lambda$, $\sigma_b \simeq 2\pi r_c L^2/\lambda$ (Kraus 1988), and the backscatter efficiency $\epsilon_b = \pi L/\lambda$ greatly exceeds unity. (Here ϵ_b is the ratio of the radar cross section to the physical cross section.)

In practice the presence of the radial halo of plasma outside of r_c modifies the dielectric constant and the cylinder at r_c is partially defocussed by the refractive effects. This tends to reduce the radar cross section by a factor of ~ 2 for most conditions (Poulter & Baggaley 1977).

3. EAS ionization densities

3.1. Longitudinal ionization

There are many years of development of the theory of EAS production. The most accurate treatments of the evolution of the electron density in the shower require numerical simulations, but there are a number of parameterizations available that yield results accurate enough for our needs. Here we use the analytical model due originally to Kamata & Nishimura (1958), and Greisen (1965). In this model the longitudinal (along-track) development of the shower at a depth d is parameterized by its *age* s:

$$s(d) \;=\; \frac{3d/X_0}{d/X_0 + 2\ln(E/E_{crit})} \tag{4}$$

where $E_{crit} = 86$ MeV for electrons in air, and $X_0 = 36.7$ gm cm^{-2} is the electron radiation length in air. The total number of charged particles (virtually all electrons & positrons) is then approximated by

$$N_e \;\simeq\; \frac{0.31\exp((d/X_0)(1-1.5\ln s))}{\sqrt{\ln(E/E_{crit})}}\,. \tag{5}$$

Although this approach does not account for any of the large fluctuations that are possible in high energy air showers, it describes the average behavior reasonably well. In particular, although it can fail to predict accurately the depth of the shower maximum, it is able to predict more closely the total number of charged particles in a shower which is important in determining the net ionization.

3.2. Transverse ionization density

The transverse charged particle densities are described in a similar fashion, also parameterized by the age of the shower (Bourdeau 1980):

$$\xi_e = \frac{N_e}{2\pi r_{mol}^2 s_m^2} \frac{\Gamma(4.5-s)}{\Gamma(s)\Gamma(4.5-s)} \left(\frac{r}{r_{mol} s_m}\right)^{s-2} \left(1+\frac{r}{r_{mol} s_m}\right)^{s-4.5} \quad (6)$$

where Γ is the gamma function, and $s_m = 0.78 - 0.21s$. The Moliere radius can be approximated as $r_{mol} = 2.12 \times 10^7 X_0 (E_{crit}\ \rho_{air})^{-1}$ cm. The calculated density ξ_e is in units of charged particles per unit area, but can be considered to be the volume density in a slab transverse to the shower since the shower thickness is negligible compared to its length.

To convert these densities to ionization densities we assume $\rho_e = Y\xi_e$ where the ion pair yield $Y \simeq 45/\beta^2$ cm^{-1} for electrons of velocity β, below $E_e \sim 10$ MeV. Fig. 1 shows curves of calculated ionization line densities for several EAS of different primary energies over the range of $10^{19} - 10^{21}$ eV. The showers are assumed to be propagating horizontally at an altitude of 10km, and the shower parameters are corrected for the lower air density at this altitude. The bottom axis shows the along-track distance corresponding to the depth shown along the top axis. As noted above, the line densities at these energies correspond to typical line densities of radio meteors, which are detected at heights of 80-120 km.

In Fig. 2, we show the lateral ionization density distributions near shower maximum for the same 5 EAS presented in Fig. 1 (solid lines). Included also are curves of the effective plasma frequency corresponding to the density at each radial distance (dashed lines). Given the uncertainty in the accuracy of the analytical model for EAS development at very small core radii (cf. $r < 20$ cm), the implied highest radar frequencies that will undergo total reflection are in the range of 10-50 MHz, with a strong dependence on the primary energy.

3.3. Diffusion of the column & the echo decay time

The duration of meteor radar echoes has been modelled and studied in detail for many decades (cf. Hanbury Brown & Lovell 1957; Kaiser 1968; Kaiser et al. 1969; Jones & Jones 1990; Jones 1991). The power of a meteor radar echo is found in the underdense regime to decay exponentially with a time constant $\tau_m = \lambda^2/(32\pi^2 D_i)$ where D_i is the ambipolar (or ion neutral) diffusion coefficient. At the altitudes that meteors are observed with radar, $D_i \simeq 1 - 10$ m^2 s^{-1}, and the typical decay times for underdense trails are thus in the tens of ms for frequencies in the VHF regime.

To estimate diffusion effects at the lower altitudes of EAS ionization columns, we note that $D_i \propto T\nu_i^{-1}$ where T is the kinetic temperature and ν_i the collision frequency (cf. Buonsanto et al. 1997). Thus at 10 km altitude, the diffusion coefficient is much smaller, $D_i \sim 5$ cm^2 s^{-1}, due mainly to the much higher collision frequency at lower altitudes. The implied time constant,

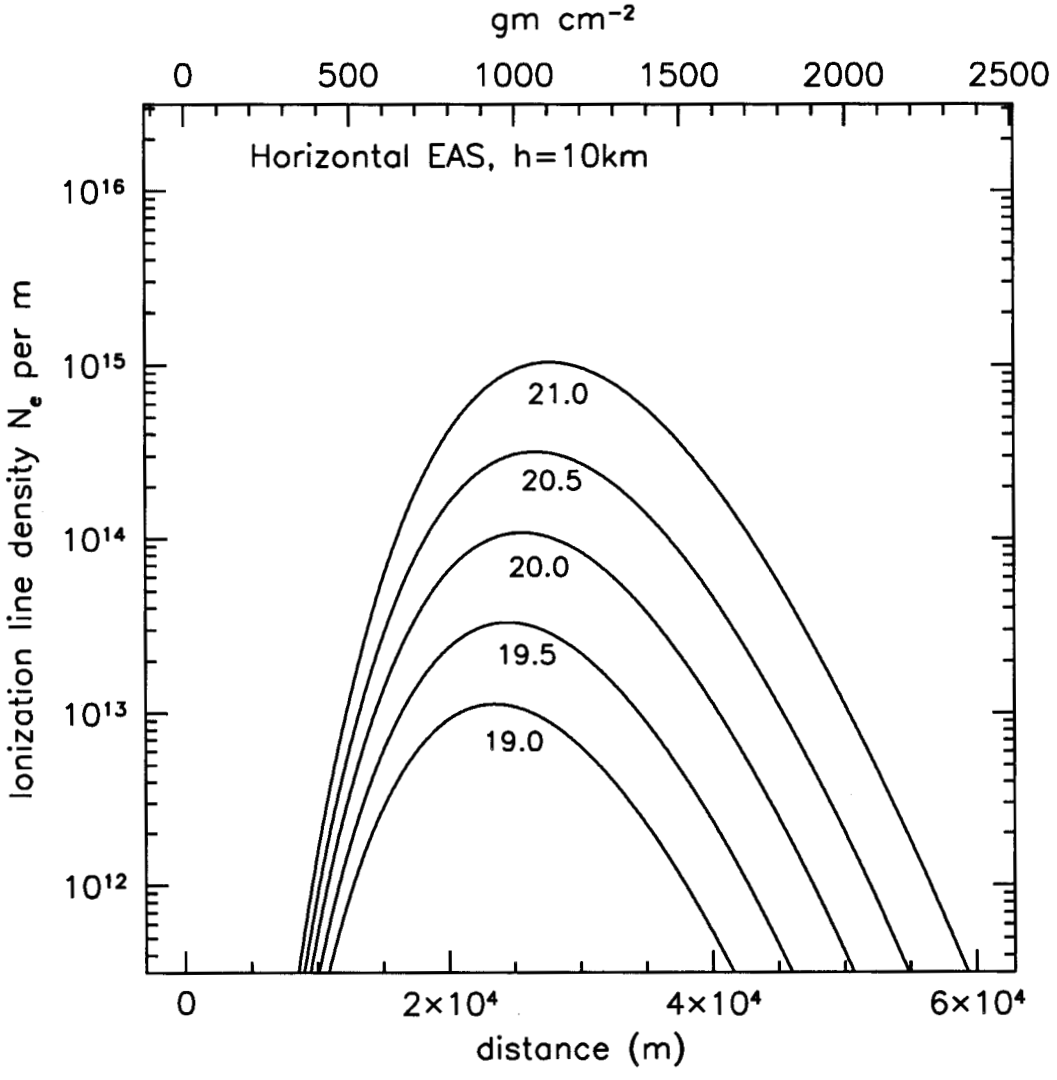

Fig. 1.— Electron ionization line density for 5 showers of energies in the 10^{19} to 10^{21} eV range. Such line densities are quite similar to those of radio meteors.

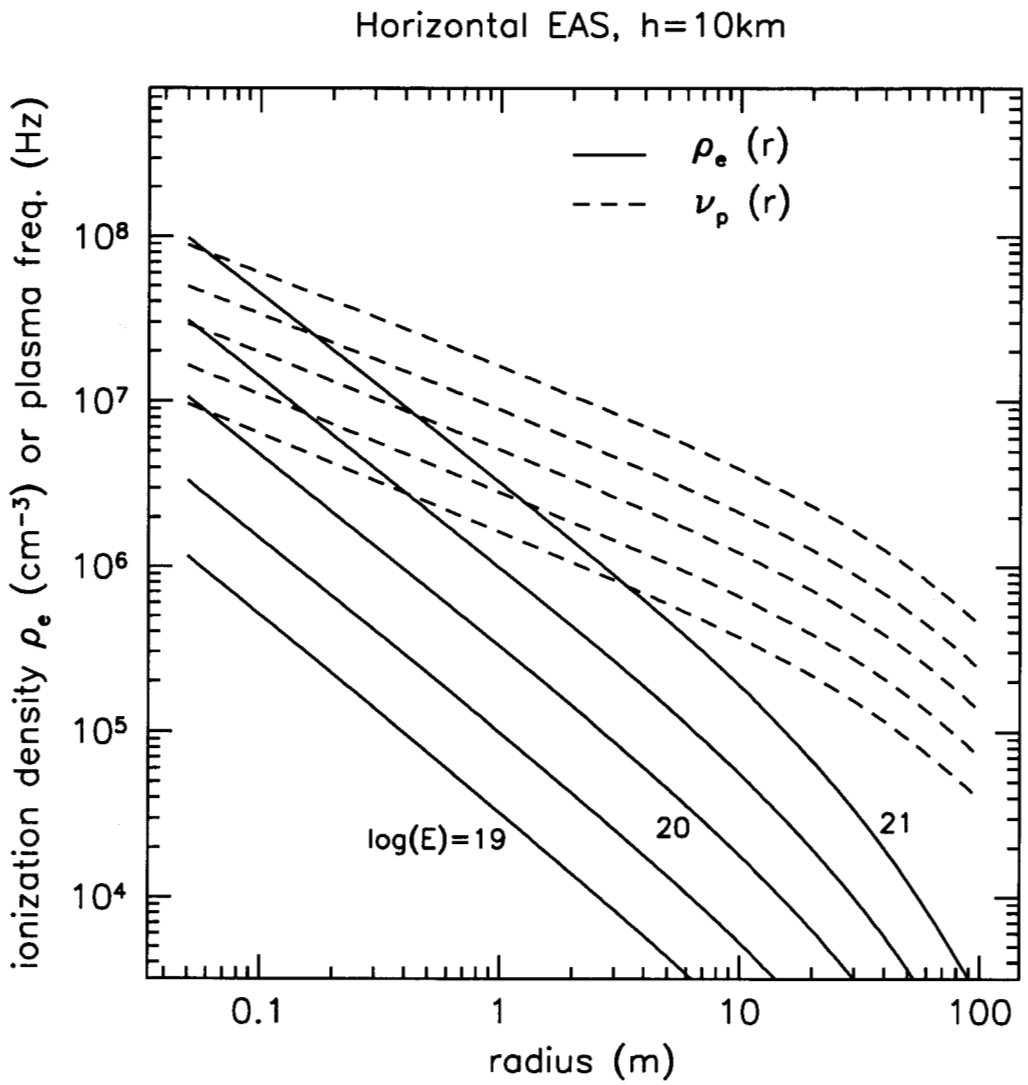

Fig. 2.— Radial dependence of the ionization density for the same showers presented in the previous figure. Also shown is the radial dependence of the plasma frequency for each case.

assuming diffusion progresses in the same manner for EAS as for meteor ionization columns, is $\tau_{eas} \simeq 60$ s for $\lambda = 3$ m. This value appears improbably long, and other effects, such as ion recombination or wind turbulence will act to reduce the ionization density on shorter time scales, but this exercise does highlight the fact that EAS ionization columns should be relatively long-lived events from the point of view of radar echoes.

4. Predicted radar return power from EAS

Radar return power P_r is described in terms of a model where the radiation is emitted from an antenna with peak transmitted power P_t and directivity gain $G = 4\pi\Omega_A^{-1}$, where Ω_A is the solid angle of the main beam of the antenna. The radiation is assumed to then scatter from objects in the field of view and be re-radiated isotropically in the frame of the scatterer, producing a R^{-4} dependence in the returned power as a function of range. Deviations from isotropic scattering are thus absorbed into the effective radar backscatter cross-section σ_b, which can be larger or smaller than the physical cross-section of the object. In addition any real transmitting and receiving system will have less than unity efficiency, which we designate here as η. The radar equation under these conditions is

$$\frac{P_r}{P_t} = \sigma_b \eta \frac{G^2 \lambda^2}{(4\pi)^3 R^4} . \tag{7}$$

Here we are assuming that the transmitting and receiving antennas are identical, and we are neglecting for the moment any polarization effects.[1]

Given equation 7, the problem of determining the detectability of EAS-initiated ionization columns reduces to that of determining the effective radar cross section σ_b for a given choice of operating radar frequency, and the noise power of the specific radar in use. The noise power is given by $P_N = kT_{sys}\Delta f$, where T_{sys} is the system noise temperature, k is Boltzmann's constant, and Δf the effective receiving bandwidth, assumed here to be matched to the transmitting bandwidth. Almost all modern radar systems now use what is known as *pulse compression*, a method which allows the receiver bandwidth, and thus the noise power, to be minimized (cf. Wehner 1987). In practice this approach is implemented by effectively dispersing a band-limited pulse with bandwidth Δf_0 through a filter, transforming it into a frequency chirp which spans the original bandwidth, but now has a duration Δt. The receiver then uses an inverse filter to de-disperse the received pulse. The effective bandwidth is thus $\Delta f = (\Delta t)^{-1}$, but the range resolution of the full bandwidth Δf_0 is recovered.

Combining the noise power equation above with equation 7, the signal-to-noise ratio (SNR)

---

[1]This equation is also derived strictly under conditions where the received radiation is in the far-field, that is, where $R > 2D^2/\lambda$ where D is the largest projected dimension of the scattering target. In our case, this is not generally satisfied, since the length of the ionization columns can be tens of km. However, we have already accounted for these Fresnel zone effects by limiting our analysis to the first Fresnel zone as noted above.

of the received power is

$$\frac{P_r}{P_N} = \sigma_b P_t \eta \frac{G^2\lambda^2}{(4\pi)^3 R^4} \frac{1}{kT_{sys}\Delta f} . \quad (8)$$

Evaluating equation 8 for a nominal choice of parameters gives the SNR per received radar pulse per square meter of radar cross section:

$$\frac{S}{N} = 3.3 \left(\frac{\sigma_b}{1\ \mathrm{m}^2}\right) \left(\frac{P_t}{1\ \mathrm{kW}}\right) \left(\frac{\eta}{0.1}\right) \left(\frac{G}{10}\right)^2 \left(\frac{\lambda}{3\ \mathrm{m}}\right)^2 \left(\frac{R}{10^4\ \mathrm{m}}\right)^{-4} \left(\frac{T_{sys}}{10^3\ \mathrm{K}}\right)^{-1} \left(\frac{\Delta t}{10\ \mu\mathrm{s}}\right) . \quad (9)$$

We note that the values chosen here represent a modest radar system; in particular the peak power of 1 kW is low by current standards, and the directivity $G \simeq 10$ represents a relatively low-gain antenna. The system temperature $T_{sys} = 1000$ K is realistic for 100 MHz however, since the brightness temperature of the sky is quite high at these frequencies.

Radar systems also routinely use repetitive pulsing to increase SNR, which then grows as $N_p^{1/2}$ where N_p is the number of pulses that are averaged. In the case of an EAS, the number of repetitions is limited by the diffusion time of the ionization column. Based on the behavior of meteor trails and the analysis presented above, this time could several seconds, and the shower ionization density is likely to be almost unchanged over perhaps hundreds of ms, allowing for $N_p \sim 100$ or more.

4.1. Radar cross section: low-frequency/overdense case

At radar frequencies below the plasma frequency of the ionized core of the EAS, the radar cross section is comparable to that of a metal cylinder, as noted above, with $\sigma_b = \kappa 2\pi r_c L^2 \lambda^{-1}$ where $\kappa \leq 1$ is an efficiency factor that accounts for defocussing losses and polarization mismatch. For long tracks, the Fresnel zone length L can be expresses in terms of the distance R, and thus $\sigma_b = \kappa\pi r_c R$. The critical radius at a given wavelength and EAS cascade energy E_c can be empirically approximated by

$$r_c = \left(\frac{f}{10\ \mathrm{MHz}}\right)^{-1.6} \left(\frac{E_c}{10^{20}\ \mathrm{eV}}\right) \mathrm{m}, \quad (10)$$

based on the shower approximations used above, and the radar cross section in this case becomes

$$\sigma_b^{od} = 3100 \left(\frac{\kappa}{0.1}\right) \left(\frac{f}{10\ \mathrm{MHz}}\right)^{-1.6} \left(\frac{E_c}{10^{20}\ \mathrm{eV}}\right) \left(\frac{R}{10^4\ \mathrm{m}}\right) \mathrm{m}^2 \quad (11)$$

which shows that, at low frequencies the effective cross section of a EAS at these energies is quite large.[2] Comparison with equation 9 above shows that such events should be easily detectable with a modest radar system. For example, at 30 MHz ($\lambda = 10$m), where the sky brightness temperature

[2]For example, a modern jumbo jetliner has $\sigma_b \simeq 100$ m^2 (Balanis 1997).

is $\sim$ 12000 K, $\sigma_b \simeq 50$ m^2 for an EAS with $E_c = 10^{19}$ eV, giving a SNR $\simeq 160$ per 10μs pulse at $P_t = 1$kW and a shower range of 10km. Clearly a fully optimized system would not be limited to merely detecting and ranging such events but could also characterize the ionization profile in detail. However, the rapid increase in sky brightness temperature below 30 MHz (Kraus 1988) makes it difficult to take advantage of the large cross sections in the overdense case for showers below $\sim 10^{20}$ eV.

4.2. Radar cross section: high-frequency/underdense case

When either the frequency is high enough or the ionization density low enough that there is effectively no region of the column where the critical density obtains, the radar return is due to Thomson scattering of the free electrons in the column, modulated by the phase factor associated with the physical extent of the ionized region. The power factor due to a given line density α_0 must fall within the range $\alpha_0 \leq \alpha_{eff} \leq \alpha_0^2$, corresponding to the incoherent, partially coherent, and fully coherent regimes as previously noted. We express this in terms of the normalized power factor Φ:

$$\alpha_{eff} = \alpha_0[1 + \alpha_0\Phi(f)] \tag{12}$$

which reduces to the incoherent case in the limit $\Phi \rightarrow 0$.

To evaluate $\Phi(f)$, we have applied equation 3 to the electron densities determined by our shower parameterization equation 6. Since the densities are approximately constant along the column, the volume element $d^3\mathbf{r} = dLd^2\mathbf{r}$, where dL is a longitudinal differential, and $d^2\mathbf{r}$ is an area element. We can then use a two-dimensional Fourier transform of the density distribution, which is cylindrically symmetric, to estimate the power loss factor. Since L is approximately constant in the region of shower maximum, the integral over dL yields the Fresnel zone length L.

Fig. 3 shows the results of this for two horizontal showers at altitudes of 5 and 10 km, for $E_c = 10^{20}$ eV. We have also investigated the behavior at other energies in this regime and found the results to be insensitive to energy over the range $10^{19} - 10^{21}$ eV. However, it is clear that there are strong dependencies in Φ on both radar frequency and shower altitude. For the two cases shown we have included fitted power laws $\Phi(f; 5km) = 1.28 \times 10^7\ f^{-1.15}$ and $\Phi(f; 10km) = 8.55 \times 10^{10}\ f^{-1.84}$ which are individually accurate to about 20% over the range from 10 MHz to 0.4 GHz. We have not attempted to produce a more general form for these empirical relations, since the general case involves showers at inclined angles for which the assumption of longitudinal homogeneity is not satisfied.

Given a value for Φ, we can calculate a modified value for σ_b in equation 1, based on $N_{e;eff} = \alpha_{eff}L$. Thus we now have

$$\sigma_b^{ud} = \alpha[1 + \alpha\Phi(f)]\frac{\lambda R}{2}\,\sigma_{Th} \tag{13}$$

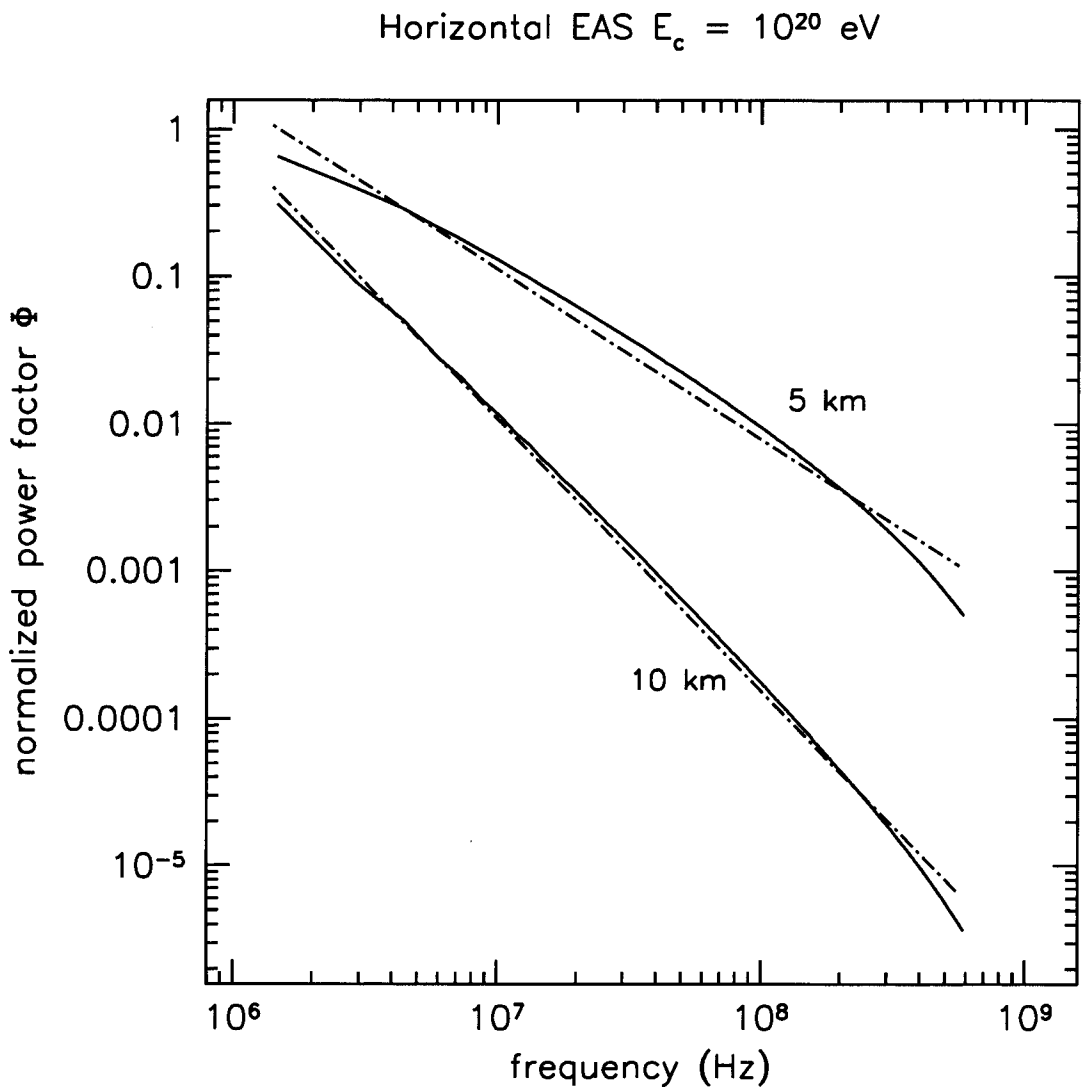

Fig. 3.— Normalized power loss factor due to loss of coherence for two horizontal E = 10^{20} eV showers at heights of 5 and 10 km.

which reduces to equation 1 in the limit of low frequencies and large values of α. Evaluating this modified cross section for its energy and frequency dependence, we can derive an expression for the case of a horizontal EAS at $h = 10$ km:

$$\sigma_b^{ud} = 50 \left(\frac{f}{30 \text{ MHz}}\right)^{-2.85} \left(\frac{E_c}{10^{20} \text{ eV}}\right)^2 \left(\frac{R}{10^4 \text{ m}}\right) \text{ m}^2 . \quad (14)$$

It is notable that this equation has both a steeper frequency dependence than the overdense case, and a stronger dependence on primary energy. Thus a system which is not signal-to-noise limited in its detection sensitivity may wish to move to higher frequencies if the goal is estimating the total energy of the observed EAS.

4.3. Caveats

We note that, due to self-imposed limitations of scope, a number of effects have not been treated in our analysis. We list several of these here.

EAS structure. The actual development of real air showers is complex and often involved significant departures from the average profiles used here. Such fluctuations may themselves yield stronger or weaker returns than expected due to the strongly non-linear dependence of the radar cross section on the ionization density.

Geomagnetic effects. We have neglected geomagnetic charge separation in the shower development. Although this is an important effect in determining the detailed shower structure, it depends greatly on the shower direction with respect to the magnetic field. Its effect on the radar cross section would also depend on the angle of observation and the treatment of this complex interaction is beyond our scope at present.

Landau-Pomeranchuk-Migdal (LPM) effect. We have neglected the LPM effect in the showers considered here. This effect, which produces an initial elongation of the shower, is important at the energies discussed and should be accounted for in a more detailed treatment. However, it affects primarily shower which interact initially through the electromagnetic rather than the hadronic channel, and thus there are still many EAS at these energies for which the approximation used is still reasonable.

Secondary Fresnel zone echoes. For simplicity we have only treated the echo from the primary Fresnel zone here. In fact, for the high SNR case, many distinct echoes may be detected from successive Fresnel zones, and these will certainly add significantly to the understanding of any detected shower.

Plasma resonance effects. We have treated the underdense case in a simplified way which neglects the possibility of plasma resonance effects. Such effects are in fact seen in meteor echoes (Poulter & Baggaley 1977) and can play an important role in enhancing the radar cross section, and in producing more complex time structure in the radar return.

Oblique Showers. We have not considered here the case of a shower for which the incident radar scatters obliquely off the ionization column, rather than at normal incidence. These cases will result in a reduced radar cross section, but the loss will scale as $(1 - \cos\theta)$, where θ is the angle between the incoming radiation and the normal to the ionization column. Thus our results are valid over a reasonably wide range of angles, of order $\theta \sim \pm 30°$.

5. Discussion

In the previous sections we have presented evidence that EAS ionization columns are well within the range of VHF radar detection for cascade energies above $\sim 10^{19}$ eV. Now we turn to a discussion of the applicability of this approach to present efforts at detection and characterization of such EAS.

For convenience we have analyzed a horizontal air shower, but such showers are of general interest, since such highly-inclined showers imply very deep initial interactions and are thus a possible signature of neutrino primaries. Generalization of our analysis to EAS at all angles is best done with a full numerical simulation.

5.1. Ground-based radar detection as part of a EAS detector array

The use of radar in conjunction with standard fluorescence detectors as a trigger could prove to be a powerful addition to these systems. For example, most of the events that triggered the first Fly's Eye detector in Utah were within a range of $R = 5$ km (Baltrusaitas et al. 1985). At this range, all of the highest energy events would produce strong radar returns with almost any system. At high signal-to-noise ratios, the timing of the return can be estimated to a precision of order $\Delta t \simeq [SNR \times \Delta f_0]^{-1}$, and thus even modest systems could produce several meter precision on the shower impact parameter.

In practice, such a system would probably require a fast phased-array, which could interrogate the approximate direction of the shower within several ms of the trigger formation. This is necessary to avoid loss of coherence to diffusion of the ionization. An alternate approach could use a high repetition rate pulsed system with a broad beam, such as a dipole pattern, and the fluorescence detector trigger could then be used to save the appropriate range bins.

Although moving to low frequencies ($f \leq 30$ MHz) is desirable from the point of view of radar

cross section, the sky temperature at these frequencies increases dramatically and would dilute most of the gain acquired in this manner. In addition interference problems will increase at low frequencies as well. It appears that the optimal frequency range is 30 – 100 MHz, as is the case for meteor observations.

5.1.1. A test case: The Auger observatory

Let us consider what is required for a radar system to enhance the planned Auger air shower array. For convenience we consider a case where each of the Auger fluorescence detectors triggers an associated radar system. The planned fluorescence detectors are required to trigger out to $\sim$ 20 km range (Dawson et al. 1997). At a frequency of 50 MHz (λ = 6 m), assuming a radar half-power beamwidth of order 5 km at 20 km (to allow for multiple Fresnel zones), we propose a moderately sparse phased-array with a diameter of order 30 m ($\sim$ 40 antennas) to interrogate the lower altitudes at 20 km distance. The implied average array gain is of order 50 for a set of half-wave dipoles (cf. Balanis 1997) with a steerable range down to elevations of $\sim$ 15°.

The required energy threshold is 10^{19} eV, and the implied radar cross section for the underdense case is 3.3 m^2 at this energy. The Fresnel zone length at this range is about 250 m for a shower at 10 km altitude, corresponding to about 10 g cm^{-2} along the track. Using a commercial VHF radar system, one can easily achieve 60 kW peak power and pulse repetition rates of 10-50 kHz for 10 μs pulses. The sky brightness temperature will lead to a system temperature of T_{sys} = 2000 K (Kraus 1988). Using these assumptions we show the SNR budget, in dBm (decibels referenced to 1 milliwatt) in Table 1.

The implied SNR in this case is of order 1300. This is not surprising, since similar radar systems are commonly used to detect comparable target areas at such ranges, at much higher frequencies. A system such as that described would be sensitive to energies down to 10^{18} eV or less, and would resolve many Fresnel zones on showers of higher energy. In addition, even nearly head-on or end-on showers will likely still retain enough effective radar cross-section to produce detectable returns at 10^{19} eV. The chosen chirp bandwidth of 1 MHz, given the estimated SNR, should allow range resolution of order 10 m or less. Note also that we have assumed only a single pulse here; averaging of multiple pulses will of course improve these values.

The advantage of such systems for planned large area arrays such as the Pierre Auger Project is that they have the potential to greatly complement the information attained by fluorescence detectors, since they share with them the property of being able to observe showers that are distant and transverse to the observation point, and further allow for active probing of the resulting ionization rather than simple passive detection. Particle counter arrays and Cherenkov detectors must by their nature be within several hundred meters of the axis to detect the shower. Fluorescence detectors and the present proposed radar approach could be combined to produce comparable levels of information for showers that are many km from the detectors.

Table 1: SNR budget of a possible EAS radar system for the Auger Observatory.

Parameter	value	+dBm	-dBm
Received Power	$\sigma_b \eta P_t G^2 \lambda^2 (4\pi)^{-3} R^{-4}$		
Peak transmit power	60 kW	77.8	
Pulse duration	10μs	...	
chirp bandwidth	1 MHz	...	
Number of repetitions	1	0.0	
Antenna gain	50	34.0	
wavelength	6 m	15.6	
σ_b at $E = 10^{19}$ eV	3.3 m^2	5.2	
range to EAS	22.4 km		-174.0
xmit/rcv efficiency	0.1		-10.0
$(4\pi)^{-3}$	5.04×10^{-4}		-33.0
Received power			-84.4 dBm
Noise power	$kT_{sys}\Delta f$		
Boltmann's constant	1.38×10^{-20} mW/K/Hz		-198.6
System temperature	2000 K	33.0	
effective bandwidth	100 kHz	50.0	
Noise power			-115.6 dBm
SNR	1300	31.2 dB	

5.2. Independent ground-based radar detection of EAS

We note here that it is possible to consider an independent radar EAS detection system that does not rely on a trigger provided by another detector. Such a system could be constructed with a single transmitting station and an array of receiving stations operating in bistatic mode, arranged in a geometry that would allow post-detection triangulation of candidate events. Synchronization of stations to the ns level over tens of km baselines is routinely done using stable clocks and GPS techniques. Each individual station would store a series of candidate EAS echoes, selected by their power and short duration, and would periodically correlate the events with the other stations. System calibration could be done using meteor echoes. Such a system, operating at 30-100 MHz, could have a range of several hundred km. The system would be sensitive to radio-frequency interference, but use of chirped pulses or other more sophisticated radar pulse shapes could be used to minimize these effects.

5.3. Space-based EAS detection with radar

We conclude this section with a discussion of the possibility of including radar detection as a complement to the fluorescence detection on a space mission such as OWL/Airwatch. The OWL/Airwatch baseline at present is to employ an optical field of view of ~ 1 sr and detect EAS fluorescence tracks with pixels giving 1 km resolution (Stalio et al. 1999) At the planned altitude in low-earth orbit of ~ 500 km, the threshold energy is expected to be $\sim 5 \times 10^{20}$ eV for a dual satellite stereoscopic version (Krizmanic et al. 1999). The necessity of stereoscopic observations has been challenged however, since it is a significant cost factor in the mission. Here we suggest that the addition of a radar system may allow for adequate information to be gathered with a single satellite.

Inspection of equation 9 shows that the radar return power varies inversely with the fourth power of the range. Thus a radar system at an altitude of 500 km (implying $R = 560$ km to EAS near the edge of the acceptance field) will require a quite different configuration than a ground-based system.

There is a significant heritage now of space-based radar systems used for both altimetry and synthetic aperture radar (SAR) imaging (cf. Hightower et al. 1993). Most of these systems are designed for use at frequencies in the microwave range from 1-10 GHz. At these frequencies the effective radar cross section is inadequate, and we are forced to consider lower frequencies. At the low end, the plasma frequency of the ionosphere limits the possibilities to frequencies above about 15 MHz, and the problem of ionospheric dispersion delays further favors higher frequencies.

This dispersive delay has the magnitude $\tau = 1.34 \times 10^{-7}\ \chi_e / f^2$ sec where χ_e is the ionospheric column density in electrons m^{-2}. A typical nighttime value is $\chi_e = 2.5 \times 10^{17}\ \mathrm{m}^{-2}$, and the delay must be doubled for a radar signal. For $f = 100$ MHz, the additional delay is about 6.7 μs. The single-pass dispersion is then given by $|\Delta\tau| = 2\tau(\Delta f / f)$ and produces an an additional $\sim 0.1\mu$s of pulse spread per MHz of bandwidth at 100 MHz for a roundtrip. Such dispersion may in fact be used to advantage since the dispersed return pulse has made a double pass through the atmosphere while noise of terrestrial origin is only single-pass. Thus some immunity to terrestrial impulsive noise may be achieved by using a receiver filter that is adapted to the known ionospheric dispersion.

One advantage of the long initial range to the targets of interest is that a longer chirp length may be used to improve the SNR. A reasonable compromise is a pulse length of $\sim 50\mu$s, which is well-matched to many radar signal processors. This pulse length would be cleanly separated from any ground clutter for a shower at 10 km altitude. Since the roundtrip time is 3.3 ms at an altitude of 500 km, a burst of 20 pulses (at 0.15 ms intervals) is possible before the transmitter must be disabled to allow for the echo returns. This sequence could thus interrogate the ionization column ~ 100 times within the first 20 ms after its formation, assuming that the fluorescence trigger can be formed within 1-2 ms. Additional pulse sequences might be used over the next 0.1-0.2 s to further improve the SNR.

Another issue of significance is the choice of antenna. At $f = 100$ MHz ($\lambda = 3$ m) the antenna size required to produce a beam comparable to the optical field of view is of order 3 m in diameter. However, it is desirable to suppress the sidelobe and backlobe response of such an antenna since the sky brightness temperature is much higher than that of the earth within the main beam. To do this will entail using a larger effective aperture and a ground-plane configuration that can suppress the backlobes. Also, since the fluorescence detector initially determines the direction to the shower, the antenna can be phased to interrogate this direction with a smaller main beam area and thus a higher gain.

The present OWL design involves a ~ 4 m diameter optical reflector. Thus a ring array of half-wave antennas outside of this could comprise a $\lambda = 3$ m phased-array with a gain of $G \simeq 50$ (half-power beamwidth of 20°), steerable over the optical field of regard. Such an array could be provided with ground plane that would reduce the system temperature to $T_{sys} = 500$K. This may or may not be possible because of constraints on the spacecraft; if not, then we expect $T_{sys} \simeq 1000$ K.

Table 2 gives a summary of the tabulated SNR for a set of radar parameters that would satisfy the requirements of a mission such as OWL. Using this system, we predict a SNR of 40 for the central Fresnel zone (~ 850 m in length near shower maximum). Range resolution of order 10-20 m would thus be achieved, and detection of additional Fresnel zones would also be likely and would then yield information on the angle with respect to the observation vector. We note that the choice of parameters described here is based on technology available off-the-shelf. In fact, integrated radar systems that meet the above requirements are available.

The significant advantage of this for OWL/Airwatch would be the availability of absolute ranges to the showers, as well as information about the total ion content that would complement the fluorescence data. One of the greatest sources of error in the fluorescence technique energy determination comes from the uncertainty in the atmospheric transmission of the fluorescence emission; radar ranges would be independent of these effects. All of these together would also lead to powerful background rejection, since false triggers produced by optical flashes that might mimic EAS fluorescence would not produce radar returns. The spatial resolution for higher energy showers would also increase rapidly as the return power increased, and could thus greatly improve the information yield for cases which would otherwise be limited by the 1 km spatial resolution of the fluorescence detectors.

Of little relevance to cosmic-ray physics, but still of great interest to meteor research, is the ability of such a system to investigate high-altitude meteor ionization trails, which would appear in the same data at ranges of order 100 km less than the EAS events. This data could be acquired during the day side portion of the OWL orbit and would thus not impact the EAS investigations. OWL/Airwatch proposals (Scarsi et al 1999) have noted the possibility of optical meteor investigations; the addition of a radar system would make a much more compelling case for OWL/Airwatch as a high altitude meteor observatory.

Table 2: SNR budget of a space-based EAS radar system for low earth orbit.

Parameter	value	+dBm	-dBm
Received Power	$\sigma_b \eta P_t G^2 \lambda^2 (4\pi)^{-3} R^{-4}$		
Peak transmit power	60 kW	77.8	
Pulse duration	50μs	...	
chirp bandwidth	1 MHz	...	
Number of repetitions	100	10.0	
Antenna gain	50	34.0	
wavelength	3 m	9.6	
σ_b at $E = 3 \times 10^{20}$ eV	815 m^2	29.1	
range to EAS	560 km		-230.1
xmit/rcv efficiency	0.1		-10.0
$(4\pi)^{-3}$	5.04×10^{-4}		-33.0
Received power			-112.6 dBm
Noise power	$kT_{sys}\Delta f$		
Boltmann's constant	1.38×10^{-20} mW/K/Hz		-198.6
System temperature	500 K	27.0	
effective bandwidth	20 kHz	43.0	
Noise power			-128.6 dBm
SNR	39.8	16.0 dB	

6. Conclusions

We have demonstrated that, using standard models for the average behavior of extensive air shower development, the resulting ionization is straightforward to detect using radar techniques in the VHF frequency range (30–100 MHz), for primary energies greater than about 10^{19} eV. We estimate that a relatively modest ground-based system, utilizing a trigger from an existing air shower array such as the Fly's Eye HiRes system in Utah, could estimate ranges to these showers with a precision of 10-20 m. More sophisticated systems may be able to provide detailed information on shower structure for arrays such as the Auger Observatory, and possibly even work as standalone detectors for such showers.

We have also analyzed the potential for using such a system on a space mission such as OWL/Airwatch, and we find that a VHF radar system appears capable of detecting and ranging showers of energies above $\sim 10^{20}$ eV with a precision of ~ 20 m, and a spatial resolution at least as

Scarsi, L. et al., 1999, Proc. 26th Int. Cosmic Ray Conf., eds. Kieda, Dingus & Salamon, (Univ. Utah: Salt Lake City) vol 2, 384.

Stalio, R. et al. 1999, Proc. 26th Int. Cosmic Ray Conf., eds. Kieda, Dingus & Salamon, (Univ. Utah: Salt Lake City) vol 2, 403.

Wehner, D. R., 1987, *High Resolution Radar*, (Norwood, MA: Artech House).

good as the planned optical imaging system, and which improves significantly for higher energies as the echo return power grows.

We thank David Saltzberg and George Resch for useful discussion and comments. This research has been performed at the Jet Propulsion Laboratory, California institute of Technology, under contract with the National Aeronautics and Space Administration.

REFERENCES

Balanis, C. A., 1997, *Antenna Theory*, 2nd edition, (New York: Wiley & Sons).

Baltrusaitis, R. M., Cady, R., Cassiday, G. L., Cooper, R., Elbert, J. W., Gerhardy, P. R., Ko, S., Loh, E. C., Salamon, M., Steck, D., & Sokolsky, P., 1985, NIM A240, 410.

Bourdeau, M. F., et al., 1980, J Phys. G: Nucl. Phys. 6, 901.

Buonsanto, M., Sipler, D. P., Davenport, G. B., & Holt, J. M., 1997, J. Geophys. Res. 102 (17), 267.

Capelle, K.S., Cronin, J.W., Parente, G., & Zas, E., 1998, Astropart. Phys. 8, 321.

Dawson, B.R. et al., 1997, Proc. 25th International Cosmic Ray Conf., Durban, OG 10.6.16.

Greenhow, J. S., 1952, Proc. Phys. Soc. B, 65, 169.

Greisen, K., 1965, in Prog. Cosmic Ray Physics vol. III, J.G. Wilson ed., (North Holland: Amsterdam) 1.

Guérard, C. K., et al. 1998, Proc. Workshop Front. Astroph. & Part. Physics, Vulcano, Sicily.

Hanbury Brown, R., & Lovell, A. C. B., 1962, *The Exploration of Space by Radio*, 2nd ed., (New York: Wiley).

Hightower, C. H., Brown, T., & Soon, N. Y., 1993, Proc. of the IEEE Nat. Radar Conf., 6.

Jones, J. & Jones, W. 1991, Planet. Space Sci. 19(9), 1289.

Jones, W., 1991, Planet. Space Sci. 1991, 19(9), 1283.

Kaiser, T. R., & Closs, T., 1952, Phil. Mag. 43, 1.

Kamata, K., & Nishimura, J., 1958, Suppl. Progr. Theoret. Phys. 6, 93.

Kraus, J. D., 1988, *Antennas*, 2nd ed., (New York: McGraw-Hill).

Krizmanic, J. et al., 1999, Proc. 26th Int. Cosmic Ray Conf., eds. Kieda, Dingus & Salamon, (Univ. Utah: Salt Lake City) vol 2, 388.

Lovell, A.C.B., & Clegg, J. A., 1948, Proc. Phys. Soc. 60, 491.

Poulter, E. M., & Baggaley, W. J., 1977, Journ. Atmos. Terrest. Phys. 39, 757.